Mean Free Path Effects on the Experimentally Measured Thermal Conductivity of Single-Crystal Silicon Microbridges

Timothy S. English
Engineering Sciences Center,
Sandia National Laboratories,
Albuquerque, NM 87185;
Department of Mechanical Engineering,
Stanford University,
Stanford, CA 94305
e-mail: tsengli@sandia.gov;
englisht@stanford.edu

Leslie M. Phinney
Engineering Sciences Center,
Sandia National Laboratories,
Albuquerque, NM 87185
e-mail: lmphinn@sandia.gov

Patrick E. Hopkins
Department of Mechanical and
Aerospace Engineering,
University of Virginia,
Charlottesville, VA 22904
e-mail: phopkins@virginia.edu

Justin R. Serrano
Engineering Sciences Center,
Sandia National Laboratories,
Albuquerque, NM 87185
e-mail: jrserra@sandia.gov

Accurate thermal conductivity values are essential for the successful modeling, design, and thermal management of microelectromechanical systems (MEMS) and devices. However, the experimental technique best suited to measure the thermal conductivity of these systems, as well as the thermal conductivity itself, varies with the device materials, fabrication processes, geometry, and operating conditions. In this study, the thermal conductivities of boron doped single-crystal silicon microbridges fabricated using silicon-on-insulator (SOI) wafers are measured over the temperature range from 80 to 350 K. The microbridges are 4.6 mm long, 125 μm tall, and either 50 or 85 μm wide. Measurements on the 85 μm wide microbridges are made using both steady-state electrical resistance thermometry (SSERT) and optical time-domain thermoreflectance (TDTR). A thermal conductivity of 77 Wm^{-1} K^{-1} is measured for both microbridge widths at room temperature, where the results of both experimental techniques agree. However, increasing discrepancies between the thermal conductivities measured by each technique are found with decreasing temperatures below 300 K. The reduction in thermal conductivity measured by TDTR is primarily attributed to a ballistic thermal resistance contributed by phonons with mean free paths larger than the TDTR pump beam diameter. Boltzmann transport equation (BTE) modeling under the relaxation time approximation (RTA) is used to investigate the discrepancies and emphasizes the role of different interaction volumes in explaining the underprediction of TDTR measurements. [DOI: 10.1115/1.4024357]

Keywords: phonon mean free path, short pulsed laser heating, phonon spectroscopy, thermal conductivity

1 Introduction

The design and thermal management of MEMS and devices requires that accurate thermal properties be known. Specifically, the rate of thermal energy generation and conduction strongly influence device performance and reliability [1–6]. Designing around thermal requirements is complicated by the fact that thermal conductivity varies with the device materials, dimensions, processing conditions, and operating conditions (i.e., temperature). The convolution of these factors often necessitates that theoretical values or predictions of thermal conductivity be confirmed experimentally [7,8]. However, the selection of an experimental technique involves tradeoffs which are typically sample-specific. These tradeoffs are frequently driven by spatial or temporal resolution requirements necessary to probe inhomogeneous properties, and practical considerations, including access for characterization (i.e., optical or electrical) as well as device geometry and composition (i.e., complexity of the associated thermal model, meeting model assumptions while maximizing sensitivity) [9,10].

In this study, the thermal conductivity of single-crystal silicon microbridges is measured using two experimental techniques: steady-state electrical resistance thermometry (SSERT) and time-domain thermoreflectance (TDTR). The thermal conductivity of thin single-crystal silicon layers has been reported for a range of thicknesses from 20 nm [8] to 3 μm [7,11,12]. Therefore, the test structures in this study augment the data available for single-crystal silicon layers with dimensions larger than the previously described limits and at high dopant concentrations ($>10^{19}$ cm^{-3}) relevant to low power devices, while also serving as a case study for comparing the experimental techniques. In the remainder of this manuscript, emphasis is placed on understanding and quantitatively explaining the discrepancies between the reported thermal conductivity data measured by each technique.

Electrical resistance thermometry has been applied to measure the thermal conductivity of low dimensional solids (films, membranes, wires, and bridges) [13–15] in both direct [16–20] and modulated (1-omega, 2-omega, 3-omega) [21,22] current configurations. Electrical resistance thermometry is frequently chosen for its simplicity and the fact that suitable electrical contacts for testing are compatible with standard fabrication processes. Therefore, in the case that a sample is otherwise well suited for electrical testing, few modifications are required in order to package a device for thermal conductivity testing. Optical time-domain thermoreflectance is a short pulsed laser pump-probe technique which offers a noncontact method for measuring thermal conductivity. It has been applied to measure the thermal conductivity of single [23] and multilayer [24] metal films, bulk [25,26] and thin film semiconductors [27], as well as anisotropic materials [28] and superlattice structures [29]. TDTR requires a more complicated analysis procedure, yet can offer different insights compared to SSERT due to its transient, localized, and noncontact nature.

2 Microbridge Test Structures

The microbridge test structures were designed and fabricated at Sandia National Laboratories using SOI wafers sourced from

Contributed by the Heat Transfer Division of ASME for publication in the Journal of Heat Transfer. Manuscript received July 26, 2012; final manuscript received January 25, 2013; published online July 26, 2013. Assoc. Editor: Zhuomin Zhang.

Table 1 Test structures

Die number	B/NB	Widths tested (μm)	Method
1	B	50, 85	SSERT
2	B	50, 85	SSERT
3	NB	50, 85	SSERT
4	NB	85	SSERT
5	B	85	TDTR

Ultrasil. The handle layer is p-doped $\langle 100 \rangle$ silicon, with a thickness of $550 \pm 5\,\mu$m, while the buried oxide thickness is $2 \pm 0.1\,\mu$m. The device layer is $\langle 100 \rangle$ silicon with a thickness of $125 \pm 1\,\mu$m, and is p-doped (boron) at a concentration of $3.8 \times 10^{19}\,\text{cm}^{-3}$ measured by time-of-flight secondary ion mass spectrometry (SIMS). The single-crystal silicon microbridge test structure dimensions are 4.6 mm long (from the inside edge of each bond pad), 125 μm tall, and either 50 or 85 μm wide. The microbridge test structures span between bond pads to which electrical leads are wire bonded for testing purposes. The bond pads on all beams are nominally $1000 \times 1000\,\mu$m, and a $900 \times 900\,\mu$m pad on the top surface is deposited with 10, 80, and 500 nm of Cr, Pt, and Au, respectively, which provide a well adhered metal contact for wirebonding. Scanning electron microscope images show that the microbridges do not have perfectly rectangular cross sections, as nominally designed. Instead, the widths are slightly tapered ($+2\,\mu$m top, $-2\,\mu$m bottom), which is attributed to the use of high aspect ratio deep reactive-ion etching. The dopant concentration measured by SIMS was also found to be $5.4 \times 10^{19}\,\text{cm}^{-3}$ within the first 50 nm from the surface, tapering off to $3.8 \times 10^{19}\,\text{cm}^{-3}$ over the next 100 nm. Microbridges of each width were fabricated in two configurations, backside (B) and no backside (NB), where the handle layer was either left intact or removed, respectively. In cases where the backside is removed, it is etched prior to etching the device layer. A summary of the die tested in this study is provided in Table 1.

3 Steady-State Electrical Resistance Thermometry

Die selected for SSERT testing were packaged in a four-point probe configuration using 68-pin leadless chip carriers to be inserted into a Henriksen cryostat. An image of a packaged NB die is shown in Fig. 1. During all tests, the cryostat chamber was pumped below 4.6×10^{-4} Torr to minimize convective losses. The four-point probe measurements were made using a Keithley source meter and Agilent digital multimeter.

3.1 Thermal Model. SSERT measures the temperature dependent change in sample resistance, which is related to thermal conductivity through a heat diffusion equation [16]. This model assumes 1D conduction occurs along the length of the microbridge and that there are no losses to convection or radiation. During testing, a direct current is applied across the outer leads while the voltage drop is measured from the inner leads, from which resistance can be calculated as a function of applied current. By applying a series of currents, an R versus I curve is constructed. Thermal conductivity is calculated by applying a least-squares fitting routine which minimizes the difference between the predicted and measured resistance values as shown in Fig. 2. Also shown inset in Fig. 2 is the resistance of a microbridge as a function of temperature, which shows a linear temperature coefficient of resistance dependence down to low temperatures, where nonlinearities appear as predicted by Bloch-Grüneisen theory [30]. A delay time of 10 s between successive current measurements was sufficient to provide adequate time to reach steady-state for a given current, which was confirmed by the repeatability of the R versus I curve.

3.2 Corrected Temperature Calculations. The SSERT technique predicts a single thermal conductivity value for the test

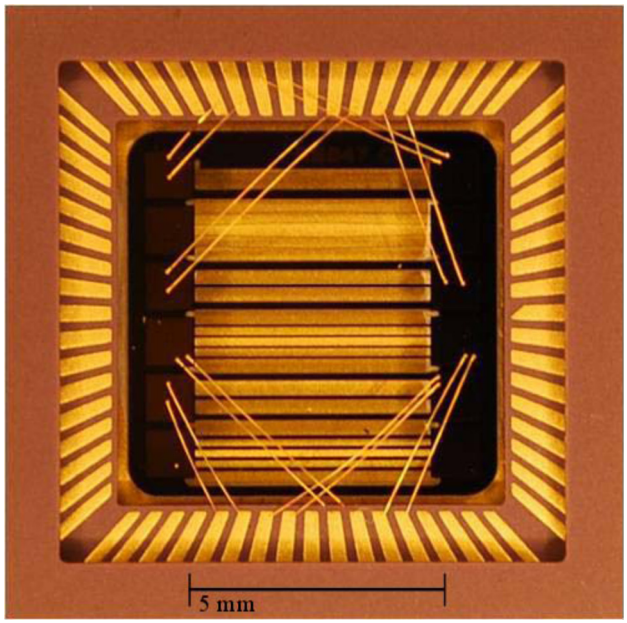

Fig. 1 Image of a packaged die (microbridges span left to right) with no backside. A subset of microbridges are wired in a four-point probe configuration with two wirebonds connected to the bondpad at each end of the structure.

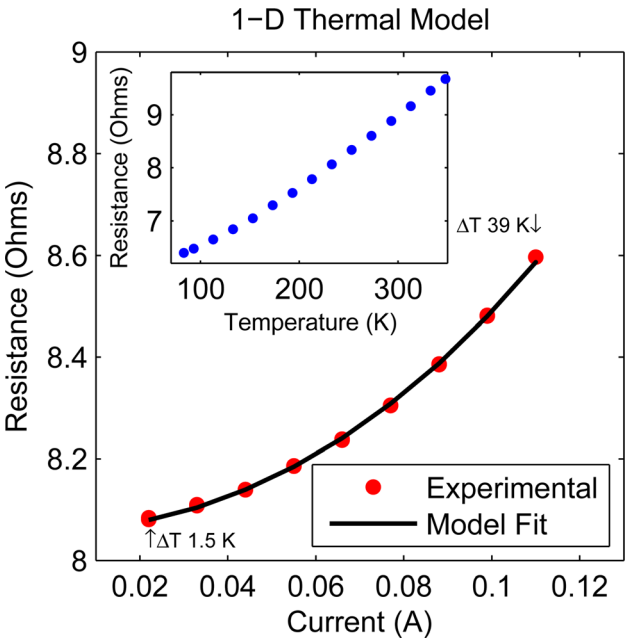

Fig. 2 Resistance measured as a function of current for an 85 μm wide microbridge at a nominal cryostat temperature of 253 K, and best fit model resistance predictions. The average temperature rise of the beam is shown for the maximum and minimum measurement currents. (Inset) Resistance of a test structure from 77 to 350 K.

structure despite the fact that the test structure is not at a uniform temperature during testing. Ideally, the temperature rise in the test structure may be assumed to be negligible if sufficiently small currents are applied. However, the test structures in this study required currents which induce significant Joule heating in order to produce a R versus I curve with sufficient curvature to fit the thermal conductivity. To account for the nonuniform temperature distribution in the beam, we calculate corrected temperatures via two methods. In method 1, the average temperature of the test

Table 2 Nominal and corrected temperatures (K)

Nominal	Method 1	Method 1% (%)	Method 2	Method 2% (%)
83	89.5	7.9	90.2	8.7
153	164.8	7.7	165.8	8.3
233	253.2	8.7	255.1	9.5
293	322.0	9.9	325.3	11.0
348	379.9	9.2	382.3	9.9

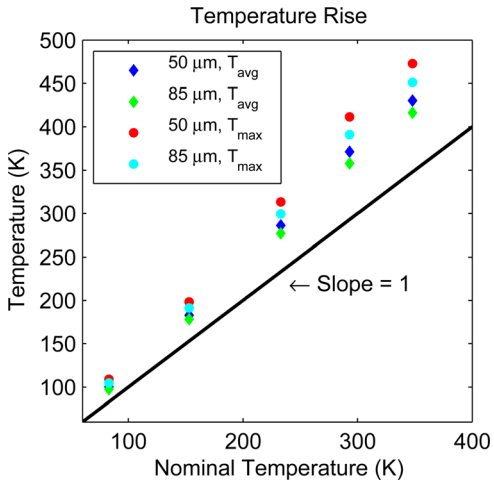

Fig. 3 Average and maximum test structure temperature for the largest applied current at several nominal (cryostat) temperatures. The departure from the solid black line (no temperature rise) increases with nominal temperature due to the decrease in the test structure thermal conductivity.

structure is calculated for each applied current over which the thermal conductivity model is fit, producing a series of average temperatures, $\bar{T}_{(I_1,I_2,I_3,\ldots)}$. We then average the series to compute an effective average temperature. Second, in method 2, the average of two values, the average microbridge temperature at the maximum applied current, and T_o, the nominal cryostat temperature, is calculated.

Table 2 compares a subset of the nominal and corrected temperatures for each method. The nonmonotonic increase in the temperature corrections is due to changes in the maximum applied current over the range of nominal temperatures tested. While method 2 may be considered an upper bound to the average temperature, method 1 is used to correct results throughout this study. The impact of heating is shown in Fig. 3, which plots the average temperature and maximum temperature for the largest applied current at several temperatures. The departure from the nominal temperature (black line), demonstrates that both the average and maximum temperature increase with nominal cryostat temperature. This is attributed to a decreasing thermal conductivity with increasing temperature, which restricts the conduction of thermal energy out of the microbridge structures. The temperature associated with all subsequent SSERT results in this study are corrected using method 1.

4 Time-Domain Thermoreflectance

Die selected for TDTR testing were coated with thin Al films via electron beam evaporation at vacuum pressures of $\sim 3 \times 10^{-7}$ Torr. The metal film acts as a transducer that relates the slight change in optical reflectance induced by the pump pulses to the change in temperature on the surface of the metal. A metal film is also necessary to ensure that the optical absorption occurs within ~10 nm beneath the surface. The thermoreflectance is monitored as a function of time and related to the thermal

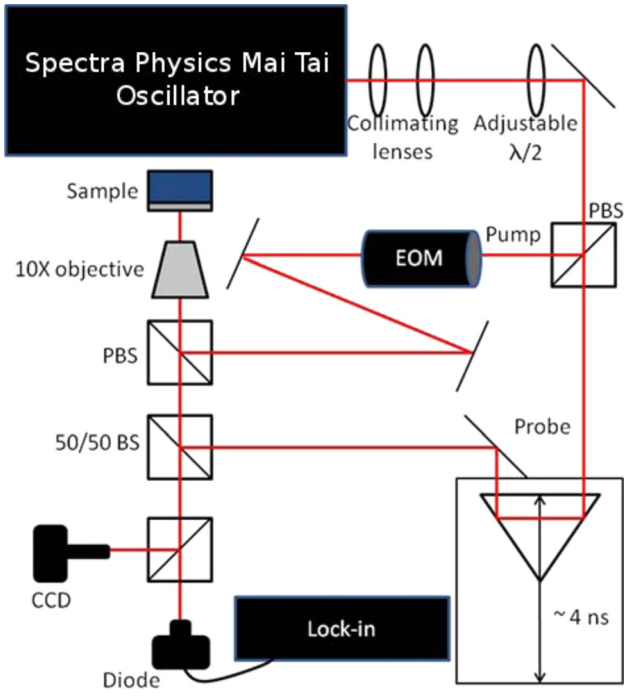

Fig. 4 Schematic of the TDTR instrument at Sandia National Laboratories

properties of interest via some form of the heat equation (as discussed below). The thickness of the metal (Al) film was 88 nm on average, as confirmed with picosecond ultrasonics [31,32].

In this work, we measure the thermal conductivity of the die as a function of temperature by mounting the samples in a liquid nitrogen cooled cryostat. Pressures in the cryostat were pumped down to ~1.0 mTorr during TDTR testing. An overview of the configuration of our specific TDTR setup at Sandia National Laboratories is discussed elsewhere and shown in Fig. 4 [26]. In short, the laser source is a Spectra Physics Mai Tai oscillator with a beam power of 300 mW at a repetition rate of 80 MHz and pulse widths of 90 fs at a wavelength of 800 nm. The pump and probe beam radii ($1/e^2$) at the sample surface are focused to ~12 μm. We modulate the pump path at $f = 11$ MHz with an electro-optic modulator and all TDTR results are calculated via an axially symmetric model [26,33] using temperature dependent heat capacity values [34,35]. This algorithm has been described in detail previously assuming a layered material geometry [28,33]. Furthermore, due to the thickness of the silicon microbridges compared to the modulation frequency of the pump, the silicon microbridges appear as semi-infinite media. This assumption is based on the fact that the thermal penetration depth during TDTR heating is on the order of $\delta \approx \sqrt{C/(\pi k f)}$, where C is the heat capacity of Si, k is the thermal conductivity, and δ is more than an order of magnitude less than the microbridge film thickness. Therefore, we note that our TDTR measurements probe the volume localized near the surface and governed by the beam geometries and thermal penetration depth.

5 Thermal Conductivity Results

The results of thermal conductivity testing are shown in Figs. 5(*a*) and 5(*b*) for the 50 and 85 μm microbridges, respectively. For comparison, the thermal conductivity of bulk, high-purity, undoped, single-crystal silicon is also shown [36]. The thermal conductivity is reduced significantly below that of the bulk reference silicon in the case of both microbridge widths, which is attributed to the high concentration of dopant (boron) atoms and associated impurity scattering. The uncertainty associated with the SSERT measurements is dominated by the application of corrected temperatures which are as large as 10% near room

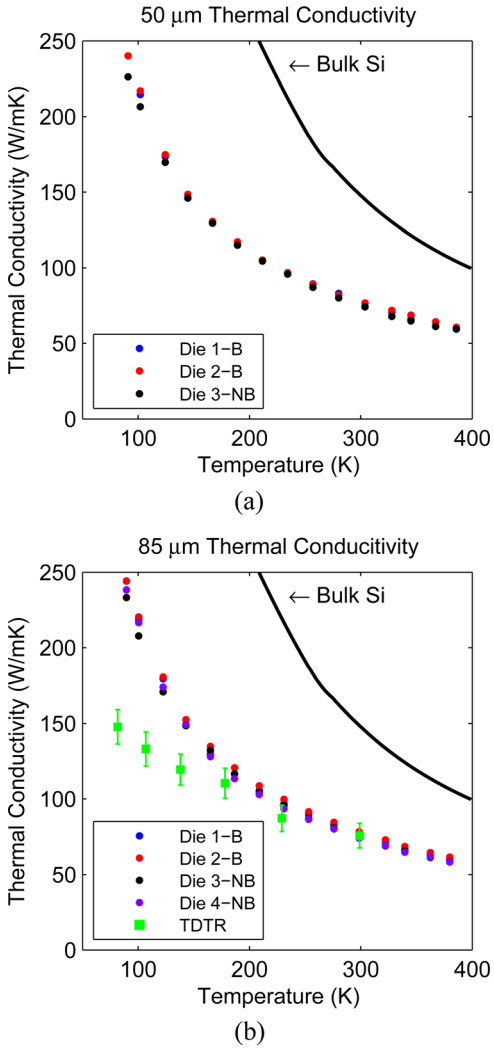

Fig. 5 Thermal conductivity plots for the 50 μm and 85 μm microbridges

temperature. The uncertainty associated with TDTR measurements is due to several sources, including uncertainties in the spot size and Al film thickness at the point of measurement on the sample surface. These uncertainties, along with the standard deviation of the mean resulting from multiple measurements at a given location on the sample, are used in calculating the error bars associated with each TDTR data point in Fig. 5(*b*).

The thermal conductivity of the 50 and 85 μm wide microbridges measured by SSERT are comparable from 80 to 350 K. The agreement amongst SSERT measurements, along with comparison to Raman thermometry [37,38] measurements and continuum multiphysics modeling not presented here, provides confidence in the SSERT measurements and repeatability across test structures. The thermal conductivity of the 85 μm wide microbridge measured by TDTR agrees with SSERT near room temperature, but diverges at lower temperatures. We consider the fact that at lower temperatures, the mean-free-path (MFP) of phonons, the primary energy carrier contributing to thermal transport, increases. However, the TDTR interaction volume defined by the beam geometries (pump and probe) and the thermal penetration depth is primarily the near-surface and nonuniform volume which includes a gradient in boron dopant concentration as measured by SIMS. Therefore, short-wavelength phonons may undergo greater scattering due to the higher concentration of impurity dopant atoms. However, at the same time, the escape of longer wavelength phonons from the interaction volume may result in a quasi-ballistic thermal transport regime with a finite ballistic thermal resistance, as has been shown in TDTR measurements on natural silicon [39,40]. Both of these phenomena would lead to lower measured thermal conductivities using TDTR, however, their relative strengths require a more detailed analysis of scattering and the spectral phonon contribution to thermal conductivity.

6 Thermal Conductivity Modeling

To assess these two factors, thermal conductivity is calculated using the Boltzmann transport equation (BTE) under the relaxation time approximation (RTA). The approach is similar to that developed by Callaway [41] and extended by Holland [42], except that an exact dispersion relation was fit from Ref. [43] along the [100] direction and used in all calculations. The thermal conductivity assuming an isotropic Brillouin zone is defined as

$$k = \frac{1}{6\pi^2}\sum_j \int_0^{q_{\max}} C_j(q) v_{g,j}^2(q) \tau_j(q) dq \tag{1}$$

where $C_j(q)$ is the specific heat capacity, $v_{g,j}(q)$ is the group velocity, and $\tau_j(q)$ is the total scattering time, where each quantity is polarization, j, and wavevector, q, dependent. Each constituent scattering mechanism is assumed to be independent and is combined using the Matthiessen's rule [44]. Scattering coefficients for phonon–phonon scattering are fit to reference experimental data for single-crystal silicon [42]

$$\tau_{p-p}^{-1}(q) = \beta \omega_j^2(q) T \exp\left(\frac{-\theta}{T}\right) \tag{2}$$

yielding coefficients $\beta = 4.4 \times 10^{-19}$ (s K^{-1}) and $\theta = 160$ (K). The impurity scattering coefficient, $A = 2 \times 10^{-43}$ (s^3), is fit from the SSERT measured thermal conductivity data at high temperatures and used in an impurity scattering rate

$$\tau_I^{-1}(q) = A\omega_j^4(q) \tag{3}$$

Similarly large values for the impurity scattering coefficient have been routinely used to model highly ($>1 \times 10^{19}$ cm^{-3}) boron doped single-crystal silicon [12,45]. Oxygen contamination and precipitation [46,47] have been proposed as one potential source of increased impurity scattering. Asheghi and coworkers [12,45] also found that these strong impurity scattering effects were more pronounced in bulk samples in comparison to highly boron doped thin films. Finally, a boundary scattering rate is introduced

$$\tau_b^{-1}(q) = \frac{v_{g,j}(q)}{2\sqrt{A_c/\pi}} \tag{4}$$

where A_c is the microbridge cross-sectional area.

For the purposes of investigating the relative difference in thermal conductivity between techniques, we consider additional scattering times which are dependent upon doping concentration. Specifically, we consider impurity scattering of the form [12,48]

$$\tau_{\text{impurity}}^{-1}(q) = \frac{nV_a^2}{4\pi v_{p,j}^2(q) v_{g,j}(q)} \left(\frac{\delta M}{M}\right)^2 \omega_j^4(q) \tag{5}$$

where n is the dopant concentration, V_a is the volume of the host atom, ω is the phonon frequency, $v_{p,j}(q)$ is the phase velocity, and δM is the difference of the substitutional impurity mass relative to the host mass (M). The introduction of strain and disruption of the local crystallographic arrangement due to dopant atoms contributes to scattering of the form [12,48]

$$\tau_{\text{strain}}^{-1}(q) = \frac{2nV_a^2}{\pi v_{p,j}^2(q) v_{g,j}(q)} Q_0^2 \gamma^2 \left(\frac{\delta R}{R}\right)^2 \omega_j^4(q) \tag{6}$$

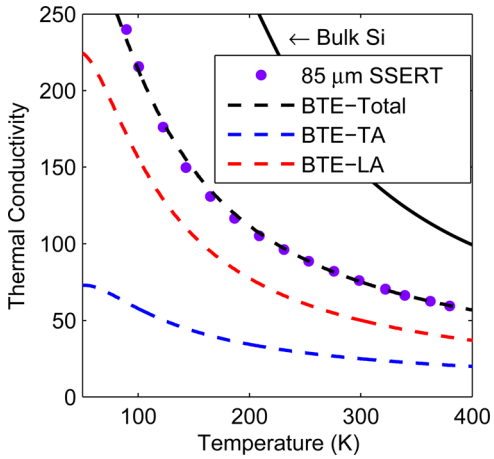

Fig. 6 Thermal conductivity calculated via the Boltzmann transport equation considering phonon–phonon, boundary, impurity, strain, and free hole-phonon scattering times with a dopant concentration $n = 3.8 \times 10^{19}\,\mathrm{cm}^{-3}$. Contributions from longitudinal and transverse acoustic phonon modes are shown.

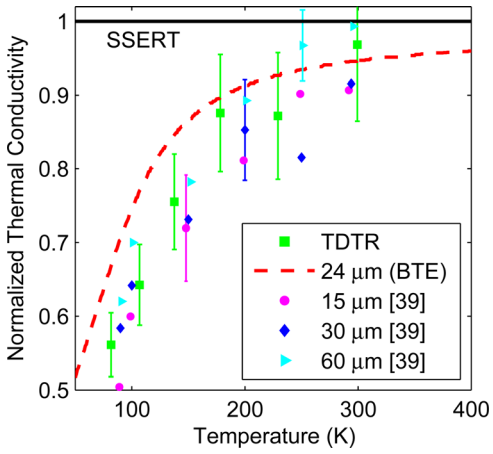

Fig. 7 Thermal conductivity calculated using the BTE and excluding phonons with MFPs larger than 24 μm, normalized to the SSERT measurements. Reduction in thermal conductivity reported in Ref. [39] for varying TDTR pump beam diameters on natural silicon are shown with select error bars from the original data.

where Q_0 is a parameter describing the anharmonicity of interactions amongst neighboring atoms of the impurity, γ is the Grüneisen constant, and δR is the difference of the substitutional impurity radii relative to the host radii R. We consider the scattering of phonons with free hole carriers, noting that the lowest measured dopant concentration in these samples ($3.8 \times 10^{19}\,\mathrm{cm}^{-3}$) is greater than the metallic transition threshold (Si:B $\approx 4 \times 10^{18}\,\mathrm{cm}^{-3}$ [49]). Thus, we assume that the free hole concentration is equal to the doping concentration, and neglect the scattering contribution of any bound holes. For wavevectors less than twice the Fermi wavevector, Q_f, we use a simplified version of the Ziman [50] scattering rate from Ref. [12]

$$\tau^{-1}_{\mathrm{free}\,e-p}(q) = \frac{(m_e E_d)^2 \hbar \omega_j(q)}{2\pi\rho\hbar^4 v_{g,j}(q)} \quad q < 2Q_f \tag{7}$$

whereas for wavevectors greater than twice the Fermi wavevector, we consider the scattering time proposed by Kosarev [51,52] for heavily doped silicon

$$\tau^{-1}_{\mathrm{free}\,e-p}(q) = \frac{185 n (m_e E_d)^2 \hbar \omega_j(q)}{\rho\hbar^3 q^5 a_b^3} \quad q > 2Q_f \tag{8}$$

where m_e is the effective mass, E_d is the deformation potential, ρ is the mass density of silicon, $\hbar$ is the reduced Planck constant, and a_b is the effective Bohr radius. We take all parameters in Eqs. (5) and (6), as well as E_d, from Ref. [12] for a similarly boron doped single-crystal silicon sample ($1 \times 10^{19}\,\mathrm{cm}^{-3}$). The effect of varying dopant concentrations is thus reflected in Eqs. (5)–(8) via E_d because it is a function of dopant concentration, $E_d \propto n^{2/3}$ [53]. The BTE calculated thermal conductivity for the 85 μm microbridge is shown in Fig. 6 using the background dopant concentration ($n = 3.8 \times 10^{19}\,\mathrm{cm}^{-3}$) as measured by SIMS and agrees with the SSERT measurements.

7 Near-Surface Dopant Effects

The former scattering times are used to investigate the impact of the increased dopant concentration in the surface region of the microbridges. We find that the magnitude of reduction in the TDTR measurements are not explained by dopant effects alone, which were evaluated for dopant concentration up to $5.4 \times 10^{19}\,\mathrm{cm}^{-3}$, the maximum value reported by SIMS characterization near the surface. This value is considered an upper bound to the effective dopant concentration within the TDTR interaction volume because the near-surface increase in dopant concentration extends roughly 150 nm from the surface. This distance is considerably less than the interaction volume defined by the thermal penetration depth (~1.2 μm). Therefore, we conclude that dopant effects alone cannot explain the large reduction in the TDTR measured thermal conductivity, especially at lower temperatures.

8 Ballistic Thermal Resistance

The impact of ballistic thermal resistance is considered within the BTE model by neglecting the thermal conductivity contribution from phonon modes whose MFPs are larger than the pump beam diameter (24 μm). The calculated reduction in thermal conductivity plotted in Fig. 7 trends closely with the TDTR data. Qualitatively, this explains the large reduction in thermal conductivity below 200 K which is not explained by the near-surface dopant gradient, or differences in intrinsic scattering mechanisms provided that both SSERT and TDTR test structures are cofabricated. Furthermore, the thermal conductivity reductions reported by Minnich et al. [39] for comparable pump diameters in natural silicon agree in trend over the reported temperature range, as shown in Fig. 7. This suggests that discrepancies in the thermal conductivity between the electrical and optical techniques in this study are due primarily to the ballistic thermal resistance measured via TDTR, with the near-surface dopant concentration playing a comparatively less important role with decreasing temperature. This is consistent with the results of Minnich et al. whose measurements were independent of modulation frequency (i.e., varying thermal penetration depth), but instead showed a pump diameter dependence. Furthermore, experimental measurements have recently demonstrated nondiffusive (ballistic) transport of long MFP phonons in silicon at room temperature [54]. These findings are consistent with the conclusion that the ballistic thermal resistance effects found in TDTR measurements in both this and previous [39] works can contribute over a wide temperature range extending from cryogenic up to even room temperatures.

9 Conclusion

The present study evaluates the role of interaction volumes and mean free path effects in the measurement of thermal conductivity via an electrical (SSERT) and optical (TDTR) technique. Measurements comparing these techniques are performed on cofabricated boron doped single-crystal silicon microbridges, eliminating

sample variations in microstructure and morphology as a factor in this study. The reported thermal conductivity values are below those of bulk undoped single-crystal silicon and attributed to the large (degenerate) doping of the microbridges. While thermal conductivity measurements by SSERT and TDTR agree near room temperature, discrepancies at lower temperatures are found to be the result of differences in the interaction volume probed by each technique.

By investigating the impact of near-surface variations in the dopant concentration and TDTR pump beam diameter on thermal conductivity, we show that the discrepancy between techniques may be explained in light of an additional ballistic thermal resistance measured via TDTR. This ballistic thermal resistance is proposed to originate from phonons with MFPs larger than the pump beam diameter. This demonstrates the importance of considering the interaction volume of experimental techniques when using measured thermal conductivity values in design or in comparing values with other experimental, theoretical, or simulated results. Electrical metrology techniques such as SSERT may be advantageous when seeking to measure the effective thermal conductivity of an entire device layer, as the measurement will include the various imperfections and inhomogenous features within the electrically active interaction volume. In this study, we believe the SSERT measurements best reflect the true intrinsic thermal conductivity of the structures, as these results are obtained in the limit of low frequency (dc measurements), or equivalently, an infinite spot size. In contrast, TDTR may be employed when a spatially localized measurement is of interest, potentially to resolve the spectral contribution of long MFP phonons to thermal conductivity. In the case of SSERT, we also investigate the need for corrected temperatures due to elevated and nonuniform test structure temperatures. Each of the highlighted issues may play into the future design of experiments, where multiple measurement techniques may be used to gain complementary information about the thermal properties and transport within a test structure.

Acknowledgment

The authors thank Edward Piekos for insights and discussion, Sandia National Laboratories SOI MEMS personnel for test structure fabrication, and Katie Francis for test structure design and layout. This work was performed, in part, at the Center for Integrated Nanotechnologies, a U.S. Department of Energy, Office of Basic Energy Sciences user facility. Sandia National Laboratories is a multiprogram laboratory managed and operated by Sandia Corporation, a wholly owned subsidiary of Lockheed Martin Corporation, for the U.S. Department of Energy's National Nuclear Security Administration under Contract No. DE-AC04-94AL85000. The United States Government retains, and the publisher, by accepting the article for publication, acknowledges, that the United States Government retains a nonexclusive, paid-up, irrevocable, world-wide license to publish or reproduce the published form of this manuscript, or allow others to do so, for United States Government purposes.

References

[1] Dwyer, V., Franklin, A., and Campbell, D., 1990, "Thermal Failure in Semiconductor Devices," Solid-State Electron., **33**(5), pp. 553–560.
[2] Cahill, D. G., Ford, W. K., Goodson, K. E., Mahan, G. D., Majumdar, A., Maris, H. J., Merlin, R., and Phillpot, S. R., 2003, "Nanoscale Thermal Transport," J. Appl. Phys., **93**(2), pp. 793–818.
[3] Liu, W., and Asheghi, M., 2005, "Impact of Phonon-Boundary Scattering and Multilevel Copper-Dielectric Interconnect System on Self-Heating of SOI Transistors," Twenty First Annual IEEE Semiconductor Thermal Measurement and Management Symposium, pp. 243–246.
[4] Pop, E., 2010, "Energy Dissipation and Transport in Nanoscale Devices," Nano Res., **3**, pp. 147–169.
[5] Phinney, L. M., Lu, W.-Y., and Serrano, J. R., 2011, "Raman and Infrared Thermometry for Microsystems," Proceedings of the ASME/JSME 8th Thermal Engineering Joint Conference (AJTEC2011)(44097).
[6] Phinney, L. M., Baker, M. S., and Serrano, J. R., 2012, "Thermal Microactuators," *Microelectromechanical Systems and Devices*, InTech, Rijeka, Croatia, pp. 415–434.
[7] McConnell, A. D., and Goodson, K. E., 2005, "Thermal Conduction in Silicon Micro- and Nanostructures," Annu. Rev. Heat Transfer, **14**, pp. 129–168.
[8] Liu, W., and Asheghi, M., 2004, "Phonon-Boundary Scattering in Ultrathin Single-Crystal Silicon Layers," J. Appl. Phys., **84**(19), pp. 3819–3821.
[9] Cahill, D. G., Goodson, K., and Majumdar, A., 2002, "Thermometry and Thermal Transport in Micro/Nanoscale Solid-State Devices and Structures," ASME J. Heat Transfer, **124**, pp. 223–241.
[10] Koh, Y. K., Singer, S. L., Kim, W., Zine, J. M. O., Lu, H., Cahill, D. G., Majumdar, A., and Gossard, A. C., 2009, "Comparison of the 3ω Method and Time-Domain Thermoreflectance for Measurements of the Cross-Plane Thermal Conductivity of Epitaxial Semiconductors," J. Appl. Phys., **105**, p. 054303.
[11] Asheghi, M., Leung, Y. K., Wong, S. S., and Goodson, K. E., 1997, "Phonon-Boundary Scattering in Thin Silicon Layers," Appl. Phys. Lett., **71**(13), pp. 1798–1800.
[12] Asheghi, M., Kurabayashi, K., Kasnavi, R., and Goodson, K. E., 2002, "Thermal Conduction in Doped Single-Crystal Silicon Films," J. Appl. Phys., **91**(8), pp. 5079–5088.
[13] Goodson, K. E., and Flik, M. I., 1994, "Solid Layer Thermal-Conductivity Measurement Techniques," Appl. Mech. Rev., **47**(3), pp. 101–112.
[14] Borca-Tasciuc, T., and Chen, G., 2004, "Experimental Techniques for Thin-Film Thermal Conductivity Characterization," *Thermal Conductivity*, T. M. Tritt, J. T. Devreese, R. P. Evrary, S. Lundqvist, G. D. Mahan, and N. H. March, eds. (Physics of Solids and Liquids), Springer, New York, pp. 205–237.
[15] Léonard, F., 2011, "Reduced Joule Heating in Nanowires," Appl. Phys. Lett., **98**(10), p. 103101.
[16] Tai, Y. C., Mastrangelo, C. H., and Muller, R. S., 1988, "Thermal Conductivity of Heavily Doped Low-Pressure Chemical Vapor Deposited Polycrystalline Silicon Films," J. Appl. Phys., **63**(5), pp. 1442–1447.
[17] Reifenberg, J., Voss, R. E., Rao, P., Schmitt, W., Yang, Y., Shojaei-Zadeh, S., Liu, W., Sadeghipour, S. M., and Asheghi, M., 2003, "Thermal Conductivity Measurements of Thin Aluminum Layers Using Steady State Joule Heating and Electrical Resistance Thermometry in Suspended Bridges," Proceedings of ASME IMECE03(42055), pp. 377–380.
[18] Yang, Y., and Asheghi, M., 2004, "A Novel Technique for In-Plane Thermal Conductivity Measurements of Electrically Conductive Interconnects and Nanostructures," Thermal and Thermomechanical Phenomena in Electronic Systems, 2004. ITHERM'04, The Ninth Intersociety Conference on, Vol. 2, pp. 564–569.
[19] Shojaei-Zadeh, S., Zhang, S., Liu, W., Yang, Y., Sadeghipour, S., Asheghi, M., and Sverdrup, P., 2004, "Thermal Characterization of Thin Film Cu Interconnects for the Next Generation of Microelectronic Devices," Thermal and Thermomechanical Phenomena in Electronic Systems, 2004. ITHERM'04, The Ninth Intersociety Conference on, Vol. 2, pp. 575–583.
[20] Phinney, L. M., Serrano, J. R., Piekos, E. S., Torczynski, J. R., Gallis, M. A., and Gorby, A. D., 2010, "Raman Thermometry Measurements and Thermal Simulations for MEMS Bridges at Pressures From 0.05 Torr to 625 Torr," ASME J. Heat Transfer, **132**(7), p. 072402.
[21] Cahill, D. G., 1990, "Thermal Conductivity Measurement From 30 to 750 K: the 3ω Method," Rev. Sci. Instrum., **61**(2), pp. 802–808.
[22] Dames, C., and Chen, G., 2005, "1ω, 2ω, and 3ω Methods for Measurments of Thermal Properties," Rev. Sci. Instrum., **76**, p. 124902.
[23] Paddock, C. A., and Eesley, G. L., 1986, "Transient Thermoreflectance From Thin Metal Films," J. Appl. Phys., **60**(1), pp. 285–290.
[24] Clemens, B. M., Eesley, G. L., and Paddock, C. A., 1988, "Time-Resolved Thermal Transport in Compositionally Modulated Metal Films," Phys. Rev. B, **37**(3), pp. 1085–1096.
[25] Koh, Y. K., and Cahill, D. G., 2007, "Frequency Dependence of the Thermal Conductivity of Semiconductor Alloys," Phys. Rev. B, **76**, p. 075207.
[26] Hopkins, P. E., Serrano, J. R., Phinney, L. M., Kearney, S. P., Grasser, T. W., and Harris, C. T., 2010, "Criteria for Cross-Plane Dominated Thermal Transport in Multilayer Thin Film Systems During Modulated Laser Heating," ASME J. Heat Transfer, **132**(8), p. 081302.
[27] Cahill, D. G., and Watanabe, F., 2004, "Thermal Conductivity of Isotopically Pure and Ge-Doped Si Epitaxial Layers From 300 to 550K," Phys. Rev. B, **70**(23), p. 235322.
[28] Schmidt, A. J., Chen, X., and Chen, G., 2008, "Pulse Accumulation, Radial Heat Conduction, and Anisotropic Thermal Conductivity in Pump-Probe Transient Thermoreflectance," Rev. Sci. Instrum., **79**, p. 114902.
[29] Capinski, W. S., Maris, H. J., Ruf, T., Cardona, M., Ploog, K., and Katzer, D. S., 1999, "Thermal-Conductivity Measurements of GaAs/AlAs Superlattices Using a Picosecond Optical Pump-and-Probe Technique," Phys. Rev. B, **59**(12), pp. 8105–8113.
[30] Bloch, F., 1930, "Zum elektrischen Widerstandsgesetz bei tiefen Temperaturen," Z. Phys. A: Hadrons Nucl., **59**, pp. 208–214.
[31] Tas, G., and Maris, H. J., 1994, "Electron Diffusion in Metals Studied by Picosecond Ultrasonics," Phys. Rev. B, **49**, pp. 15046–15054.
[32] Thomsen, C., Strait, J., Vardeny, Z., Maris, H. J., Tauc, J., and Hauser, J. J., 1984, "Coherent Phonon Generation and Detection by Picosecond Light Pulses," Phys. Rev. Lett., **53**, pp. 989–992.
[33] Cahill, D. G., 2004, "Analysis of Heat Flow in Layered Structures for Time-Domain Thermoreflectance," Rev. Sci. Instrum., **75**(12), pp. 5119–5122.
[34] Touloukian, Y. S., Powell, R. W., Ho, C. Y., and Klemens, P. G., 1970, *Thermophysical Properties of Matter—Specific Heat: Nonmetallic Solids*, Vol. 5, IFI/Plenum, New York.

[35] Touloukian, Y. S., and Buyco, E. H., 1970, *Thermophysical Properties of Matter—Specific Heat: Metallic Elements and Alloys*, Vol. 4, IFI/Plenum, New York.
[36] Ho, C. Y., Powell, R. W., and Liley, P. E., 1972, "Thermal Conductivity of the Elements," J. Phys. Chem. Ref. Data, **1**(2), pp. 279–421.
[37] Serrano, J. R., Phinney, L. M., and Kearney, S. P., 2006, "Micro-Raman Thermometry of Thermal Flexure Actuators," J. Micromechan. Microeng., **16**(7), p. 1128.
[38] Beechem, T., Graham, S., Kearney, S. P., Phinney, L. M., and Serrano, J. R., 2007, "Simultaneous Mapping of Temperature and Stress in Microdevices Using Micro-Raman Spectroscopy," Rev. Sci. Instrum., **78**(6), p. 061301.
[39] Minnich, A. J., Johnson, J. A., Schmidt, A. J., Esfarjani, K., Dresselhaus, M. S., Nelson, K. A., and Chen, G., 2011, "Thermal Conductivity Spectroscopy Technique to Measure Phonon Mean Free Paths," Phys. Rev. Lett., **107**, p. 095901.
[40] Minnich, A. J., Chen, G., Mansoor, S., and Yilbas, B. S., 2011, "Quasiballistic Heat Transfer Studied Using the Frequency-Dependent Boltzmann Transport Equation," Phys. Rev. B, **84**, p. 235207.
[41] Callaway, J., 1959, "Model for Lattice Thermal Conductivity at Low Temperatures," Phys. Rev., **113**(4), pp. 1046–1051.
[42] Holland, M. G., 1963, "Analysis of Lattice Thermal Conductivity," Phys. Rev., **132**(6), pp. 2461–2471.
[43] Weber, W., 1977, "Adiabatic Bond Charge Model for the Phonons in Diamond, Si, Ge, and α-Sn," Phys. Rev. B, **15**(10), pp. 4789–4803.
[44] Ashcroft, N. W., and Mermin, N. D., 1976. *Solid State Physics*, Saunders College Publishers, Orlando, FL.
[45] Liu, W., and Asheghi, M., 2005, "Thermal Conduction in Ultrathin Pure and Doped Single-Crystal Silicon Layers at High Temperatures," J. Appl. Phys., **98**(12), p. 123523.
[46] Fortier, D., Djerassi, H., Suzuki, K., and Albany, H. J., 1974, "Scattering of Thermal Phonons by Li-O Donors in Si," Phys. Rev. B, **9**, pp. 4340–4343.
[47] Verma, G. S., 1978, "Role of Oxygen Atoms in the Phonon Conductivity of Si Containing 5×10^{17} Oxygen Atoms per cm^3," Phys. Rev. B, **18**, pp. 5903–5905.
[48] Klemens, P. G., 1955, "The Scattering of Low-Frequency Lattice Waves by Static Imperfections," Proc. Phys. Soc., London, **68**, p. 1113.
[49] Dai, P., Zhang, Y., and Sarachik, M. P., 1991, "Critical Conductivity Exponent for Si:B," Phys. Rev. Lett., **66**, pp. 1914–1917.
[50] Ziman, J. M., 1956, "The Effect of Free Electrons on Lattice Conduction," Philos. Mag., **1**(2), pp. 191–198.
[51] Kosarev, V. V., 1971, "Scattering of Phonons by Carriers in the Field of Charged Impurities," Sov. Phys. JEPT, **33**, p. 793.
[52] Radhakrishnan, V., and Sharma, P. C., 1980, "Electron-Phonon Scattering in Li-Doped Silicon in the Intermediate Concentration Region," J. Phys. C: Solid State Phys., **13**(10), p. 2001.
[53] Ziman, J. M., 1960, *Electrons and Phonons*, 2nd ed., Oxford University Press, New York.
[54] Johnson, J. A., Maznev, A. A., Cuffe, J., Eliason, J. K., Minnich, A. J., Kehoe, T., Torres, C. M. S., Chen, G., and Nelson, K. A., 2012, "Direct Measurement of Room Temperature Non-Diffusive Thermal Transport Over Micron Distances in a Silicon Membrane," Phys. Rev. Lett., **110**, p. 025901.